


Turbulence at the edge of continuumM. A. Gallis,^{1,*} J. R. Torczynski ,¹ M. C. Krygier ,¹ N. P. Bitter,¹ and S. J. Plimpton²¹Engineering Sciences Center, Sandia National Laboratories, P. O. Box 5800, Albuquerque, New Mexico 87185-0840, USA²Center for Computing Research, Sandia National Laboratories, P. O. Box 5800, Albuquerque, New Mexico 87185-0840, USA

(Received 2 April 2020; accepted 21 December 2020; published 11 January 2021)

In typical turbulent flows, noncontinuum effects are extremely small and hence can be ignored. However, for some high-Mach-number flows, the Kolmogorov length scale is of the same order as the molecular mean free path, which could introduce noncontinuum molecular-level effects into the turbulent energy cascade. To investigate this, the compressible Taylor-Green vortex flow is simulated for near-continuum conditions using both noncontinuum molecular gas dynamics (direct simulation Monte Carlo method) and continuum computational fluid dynamics (direct numerical simulation of the Navier-Stokes equations). Although the energy-decay histories are basically the same, molecular-level fluctuations are observed to break the symmetries of the initial conditions and thereby produce different but statistically similar routes (based on velocity spectra) from the initial nonturbulent flow to the long-time turbulent flow.

DOI: [10.1103/PhysRevFluids.6.013401](https://doi.org/10.1103/PhysRevFluids.6.013401)**I. INTRODUCTION**

The concept of the turbulent energy cascade asserts that, in a statistical sense, kinetic energy generated at large length scales is transferred to progressively smaller length scales and ultimately dissipated at very small length scales [1]. In his pioneering research, Kolmogorov postulated that the behavior of turbulence at these small length scales is universal and that the Kolmogorov length, time, and velocity scales characterizing this behavior are determined solely by the energy-dissipation rate and the kinematic viscosity [1]. Subsequently, the behavior of turbulence at small length scales has been studied extensively [2–5]. In these studies, the flow is assumed to be continuum at all length scales, including the Kolmogorov length scale. The continuum assumption is reasonable when the molecular length scales and timescales are much smaller than the smallest hydrodynamic length scales and timescales. However, situations of practical interest exist for which the Kolmogorov length scales and timescales (the smallest hydrodynamic scales) are comparable to the gas molecular mean free path and mean collision time (the molecular scales).

As pointed out by Stefanov *et al.* [6], hypersonic flow over a body falls into this category. Over half a century ago, Van Driest developed theories for the turbulent shear stress on a flat plate in hypersonic flow [7] and for a sharp cone with an attached shock wave in hypersonic flow [8]. The smallest turbulent length scale in his theory is $l_w = \nu_w / \sqrt{\tau_w / \rho_w}$, where τ_w , ρ_w , and ν_w are the viscous shear stress, the density, and the kinematic viscosity at the wall conditions, and the gas molecular mean free path is $\lambda = (\mu/p) \sqrt{\pi k_B \theta / 2m}$, where μ is the dynamic viscosity, p is the pressure, θ is the temperature, k_B is the Boltzmann constant, and m is the gas molecular mass. The Van Driest theories for flow over a flat plate or a sharp cone can be used to estimate the ratio

*magalli@sandia.gov

l_w/λ for hypersonic conditions. For typical values of the skin friction coefficient at hypersonic flow conditions ($\text{Ma} \geq 4$), the ratio l_w/λ is only ~ 5 – 10 (this ratio can be even smaller if the surface is cooled below the adiabatic temperature) [7,8]. Moreover, the thickness l_s of a shock wave is often about five to ten mean free paths. Hence, the smallest length scales generated by hypersonic flow over a body can be comparable to the mean free path.

When the turbulent scales become comparable to the molecular-level scales, Tennekes and Lumley [9] and Frisch [10] state that noncontinuum molecular phenomena might be non-negligible and that the continuum assumption might need to be modified. In other words, noncontinuum effects, especially molecular-level fluctuations, which are insignificant under ordinary conditions, might become important when the Kolmogorov length scale is on the order of a few mean free paths. More specifically, the turbulent energy cascade might no longer be fully described by the overall energy-dissipation rate and the kinematic viscosity (i.e., by continuum transport), which control the small-scale motions according to Kolmogorov's first similarity hypothesis [1]. (Although Kolmogorov's first similarity hypothesis [1] has been debated [2–4], its stipulation that the small-scale motions depend on the overall energy-dissipation rate and the kinematic viscosity is generally accepted.) This dependence of turbulent energy decay on the small-scale motions motivates an investigation into how noncontinuum turbulent flow might differ from continuum turbulent flow.

To investigate this issue, compressible Taylor-Green (TG) vortex flow [11,12] is simulated using both noncontinuum molecular gas dynamics (MGD) and continuum computational fluid dynamics (CFD). For conditions ranging from continuum to near-continuum, TG flow is simulated using the direct simulation Monte Carlo (DSMC) method (the noncontinuum MGD method) and direct numerical simulation (DNS) of the Navier-Stokes equations (the continuum CFD method). Kinetic-energy and energy-dissipation histories and spectra and flow fields at selected times from the DSMC and DNS simulations are compared so that the importance of noncontinuum effects on the turbulent energy cascade can be ascertained.

II. TAYLOR-GREEN VORTEX FLOW

TG vortex flow is a canonical turbulent flow in which the generation of eddies and the corresponding cascade of energy from small to large wave numbers can be observed numerically. For a gas flow that has a (turbulent) Mach number Ma and a (turbulent) Reynolds number Re , the ratio η/λ of the Kolmogorov length scale η to the mean free path λ scales as $\text{Re}^{1/4}/\text{Ma}$ [9]. Thus, within the context of TG flow, even at a small fixed Knudsen number, the ratio η/λ can be modest (instead of large) when the Mach and Reynolds numbers jointly become large.

Compressible TG flow is initialized in a triply periodic domain $-\pi L \leq \{x, y, z\} \leq \pi L$ using fields having only a single length scale L and a single velocity scale V_0 :

$$\begin{aligned}
u &= V_0 \sin(x/L) \cos(y/L) \cos(z/L), \\
v &= -V_0 \cos(x/L) \sin(y/L) \cos(z/L), \\
w &= 0, \\
p &= p_0 + (\rho_0 V_0^2 / 16) [\cos(2x/L) + \cos(2y/L)] [\cos(2z/L) + 2], \\
\theta &= \theta_0, \\
\rho &= m p / k_B \theta.
\end{aligned} \tag{1}$$

Here, $\mathbf{u} = (u, v, w)$ is velocity, p is pressure, θ is temperature, ρ is density, $\mathbf{x} = (x, y, z)$ is position, and $T = V_0 t / L$ is nondimensional time. Thus, all of the kinetic energy is initially resident in the single wave number corresponding to L . The gas has molecular mass m and pressure, temperature, and density reference values p_0 , θ_0 , and ρ_0 , respectively, where $\rho_0 = m p_0 / k_B \theta_0$. Additionally, the gas is taken to have specific heat ratio γ and thus a sound speed $a_0 = \sqrt{\gamma k_B \theta_0 / m}$ at temperature θ_0 . Similarly, the gas is taken to have a dynamic viscosity μ_0 at temperature θ_0 . These quantities yield

TABLE I. Parameters for Taylor-Green vortex flow simulations.

Case	Description	Re	Ma	Kn	λ/δ	η/λ	η/δ
1	Incompressible	500	0.3	0.001	27.8	15.8	437
2	Subsonic	1000	0.6	0.001	27.8	9.4	260
3	Transonic	1500	0.9	0.001	27.8	6.9	192
4	Supersonic	2000	1.2	0.001	27.8	5.6	155

the Mach number $Ma = V_0/a_0$ and the Reynolds number $Re = \rho_0 V_0 L / \mu_0$, as well as the Knudsen number $Kn = \lambda/L = \sqrt{\pi\gamma/2}(Ma/Re)$.

Four cases, given in Table I, are examined using both DSMC and DNS. In all these cases, the mean density and the initial temperature are kept fixed, so the Knudsen number Kn is also kept fixed. Hence, the Reynolds number Re is proportional to the Mach number Ma . The low Knudsen number places all cases in the near-continuum regime. However, the ratio of the Kolmogorov length scale to the mean free path, η/λ , indicates that noncontinuum effects such as molecular fluctuations become more important as the Reynolds and Mach numbers are increased at fixed Knudsen number. Although desirable, smaller η/λ values cannot be investigated: Smaller Knudsen-number values are not computationally feasible, the Mach number is constrained by $Ma < 4/\sqrt{6\gamma}$ to yield positive pressure and density fields, and the Reynolds and Mach numbers are proportional ($Re \propto Ma$ at fixed Kn). In all cases, the Kolmogorov length scale η and the molecular mean free path λ are much larger than the mean molecular separation $\delta = (\rho/m)^{-1/3}$, so the numbers of molecules within volumes corresponding to these length scales are large.

Noncontinuum effects from molecular-level processes at the mean-free-path scale, especially molecular fluctuations, are not typically included in continuum CFD simulations of the Navier-Stokes equations. However, these phenomena are inherently present in MGD methods. Thus, simulations using a noncontinuum MGD method and a continuum CFD method are compared to investigate the role of noncontinuum effects on turbulence.

III. NUMERICAL METHODS

A. Direct simulation Monte Carlo

Herein, Bird’s direct simulation Monte Carlo (DSMC) method [13] of molecular gas dynamics (MGD) is used to simulate compressible turbulent TG vortex flow. DSMC uses “particles” (computational molecules) to represent a gas flow. Each particle represents a large number of real molecules. These particles move ballistically, reflect from solid boundaries, and collide stochastically in a pairwise fashion to reproduce the statistical behavior of real molecules. Particle-particle collisions are performed using the variable-soft-sphere (VSS) interaction [13]. Sampling the properties of the particles within each cell yields flow properties for each cell. Typically, the cell size and the time step are smaller than the mean free path and the mean collision time, respectively. Like most molecular methods, DSMC simulations are “noisy”: Flow quantities associated with a cell fluctuate as particles move into and out of the cell. However, DSMC fluctuations have the same characteristics as real molecular fluctuations in a gas [14]. Although traditionally DSMC has been used to simulate rarefied laminar hypersonic flows, rarefied turbulent hypersonic flows have recently begun to come within computational reach [15].

Sandia’s open-source massively parallel DSMC code SPARTA [16,17] is used to perform these simulations. SPARTA has been extensively validated for flows in the near-continuum regime [15,16]. The gas has molecular mass $m = 66.3 \times 10^{-27}$ kg; specific heat ratio $\gamma = 5/3$; and pressure, temperature, and density reference values of $p_0 = 88\,414.7$ Pa, $\theta_0 = 273.15$ K, and $\rho_0 = 1.5544$ kg/m³, which yield a sound speed of $a_0 = 307.9$ m/s. VSS molecular collisions are performed with $\omega = 0.81$ and $\alpha = 1.4$ [13]. The time step is $\Delta t = 2.5$ ps. The domain length scale is $L = 100$ μm .

The domain is subdivided into 8 billion cubical cells (2000^3) with a side length of $\pi/10 \mu\text{m}$. An average of 45 particles per cell is used, for a total of 0.36 trillion particles, where each individual particle represents approximately 16 000 real molecules. These simulations are performed on Sequoia, an IBM Blue Gene/Q supercomputer at Lawrence Livermore National Laboratory and use slightly more than half a million cores with four threads per core for 250 h.

Although the gas parameters above represent argon [13], the gas is only argonlike because the finite discretization increases the transport properties in DSMC [18]. For these simulations, the effective viscosity is found by comparing a thin-slab DSMC simulation (one layer of cells in the z direction) of the two-dimensional TG flow to the analytical expression for its kinetic-energy decay in the incompressible limit. This comparison indicates that the discretization used for these simulations leads to a dynamic viscosity of $\mu_0 = 2.8709 \times 10^{-5} \text{ Pa s}$ at $\theta_0 = 273.15 \text{ K}$, which yields the effective Reynolds numbers in Table I. At other temperatures, the viscosity behaves like $\mu = \mu_0(\theta/\theta_0)^\omega$ because VSS collisions are used [13]. The thermal conductivity is determined from the viscosity and the ideal-gas specific heat using a Prandtl number of 0.669.

B. Direct numerical simulation

Direct numerical simulation (DNS) of the Navier-Stokes equations is also used to simulate compressible turbulent TG vortex flow. The gas properties are identical to those given above for the DSMC simulations. The Sandia Parallel Aerodynamics and Reentry Code (SPARC) [19,20] is used to perform these simulations. Additionally, the code US3D [21], developed at the University of Minnesota, is used to simulate some cases to confirm that the DNS results are well resolved.

Both codes use shock-capturing finite-volume methods to achieve stability in the presence of strong shock waves and reasonably high accuracy in smooth regions of the flow. This is achieved by blending two numerical methods. The first is the modified Steger-Warming method [22], which offers good numerical stability but generates appreciable numerical dissipation. The second is the kinetic-energy-consistent central-difference scheme of Subbareddy and Candler [23], which delivers high-order spatial accuracy and lower numerical dissipation at the expense of reduced numerical stability. The method switches between these two schemes using gradients in the Mach number to detect shocks and apply the stabilizing modified Steger-Warming fluxes in those regions. The result is an overall scheme that has good accuracy in smooth parts of the flow and is robust to shock waves. Time advancement is accomplished using a third-order explicit Runge-Kutta method with a Courant-Friedrichs-Lewy number of 0.5 to determine the time step.

SPARC DNS results on 512^3 and 1024^3 meshes are compared with US3D DNS results on 400^3 and 600^3 meshes. The corresponding dissipation rates are almost indistinguishable for $\text{Ma} = 0.3\text{--}0.9$, and only slight differences are observed for $\text{Ma} = 1.2$. Thus, the SPARC results on the 512^3 mesh are deemed to be sufficiently converged for the purposes herein.

IV. RESULTS

A. Energy decay

Figures 1 and 2 present results for the kinetic energy and its corresponding dissipation rate from the DSMC and DNS simulations of all four cases as functions of time. The energy histories from both methods are in good agreement for all four cases, exhibiting the same plateaus from $T = 0$ to $T = 4$ followed by rapid decays at longer times. The dissipation histories show the fine details of the energy decay more clearly. The DSMC and DNS results are in good agreement over the entire time during which energy dissipation is significant. For all four cases, both methods have the same rapid increases from $T = 0$ to $T = 8$, the same plateaus from $T = 8$ to $T = 12$, the same maxima in this interval, the same rapid decreases from $T = 12$ to $T = 17$, the same slow decreases from $T = 17$ to $T = 20$, and the same oscillations throughout the duration. Cases 1–3 show good agreement over the entire duration of $0 \leq T \leq 20$, but case 4 shows some slight differences after $T = 10$. However, even at these later times, the DSMC and DNS results agree fairly closely.

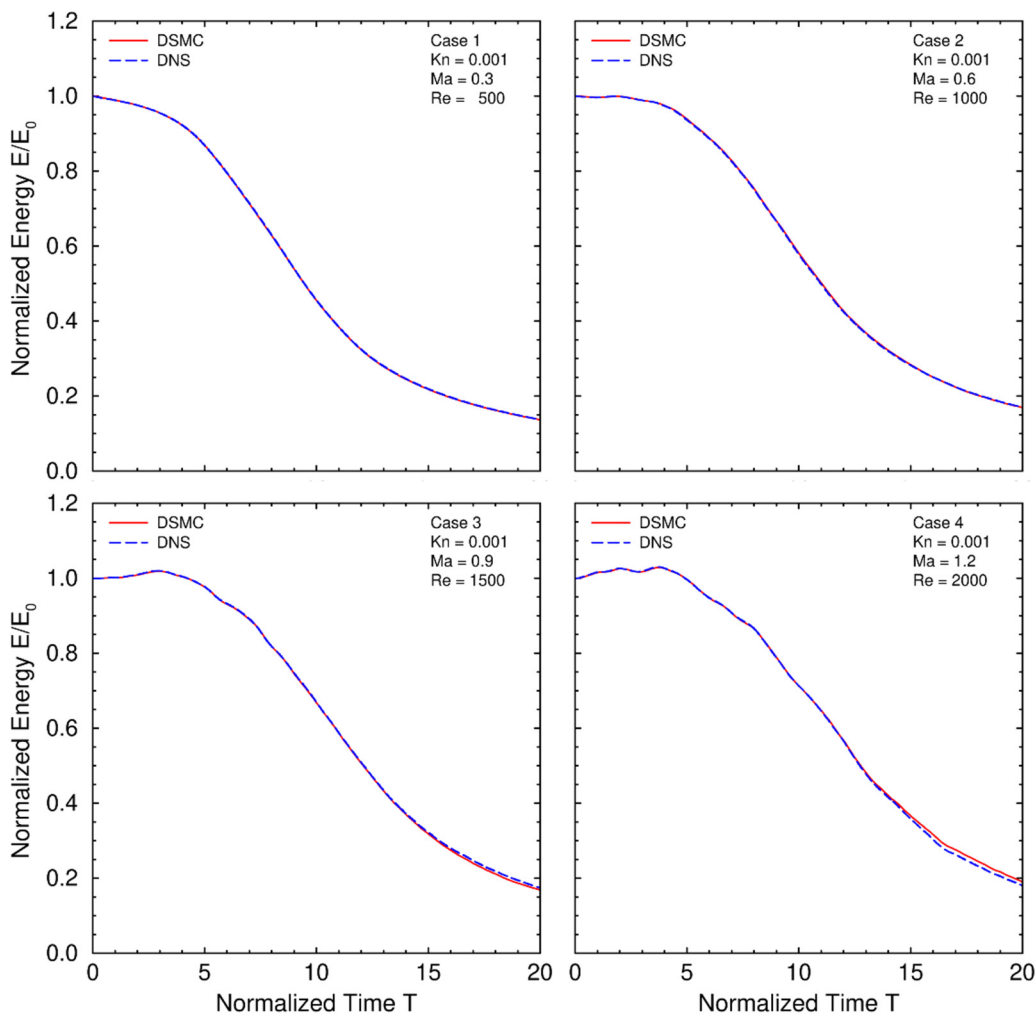


FIG. 1. Energy versus time from DSMC and DNS.

Figure 3 presents the normalized three-dimensional spectra from the DSMC and DNS simulations at selected times for all four cases. The raw spectra are divided by the square of the Mach number so that all cases can be displayed using the same range. Early on, energy is transferred from the initial low wave number to high wave numbers, so the energy resident in the high-wave-number region of the spectrum increases during this period. Significant energy first appears in the high-wave-number region around $T = 6$. By $T = 10$ (the maximum dissipation time), the spectra have achieved shapes that change little during the remainder of the simulations although their magnitudes decrease. This situation corresponds to the establishment of the energy cascade. The DSMC and DNS spectra for all four cases are observed to agree closely at all times, even at intermediate and high wave numbers, where the energy cascade is occurring.

Overall, the energy and dissipation histories agree well over the entire duration of the energy decay. The DSMC and DNS spectra also agree closely. Thus, the two simulation methods (non-continuum DSMC and continuum DNS) produce basically the same evolution from the initial conditions to the turbulent state. Some slight differences are observed, but this is not surprising when simulating chaotic flows with two different methods. Hence, noncontinuum molecular-level

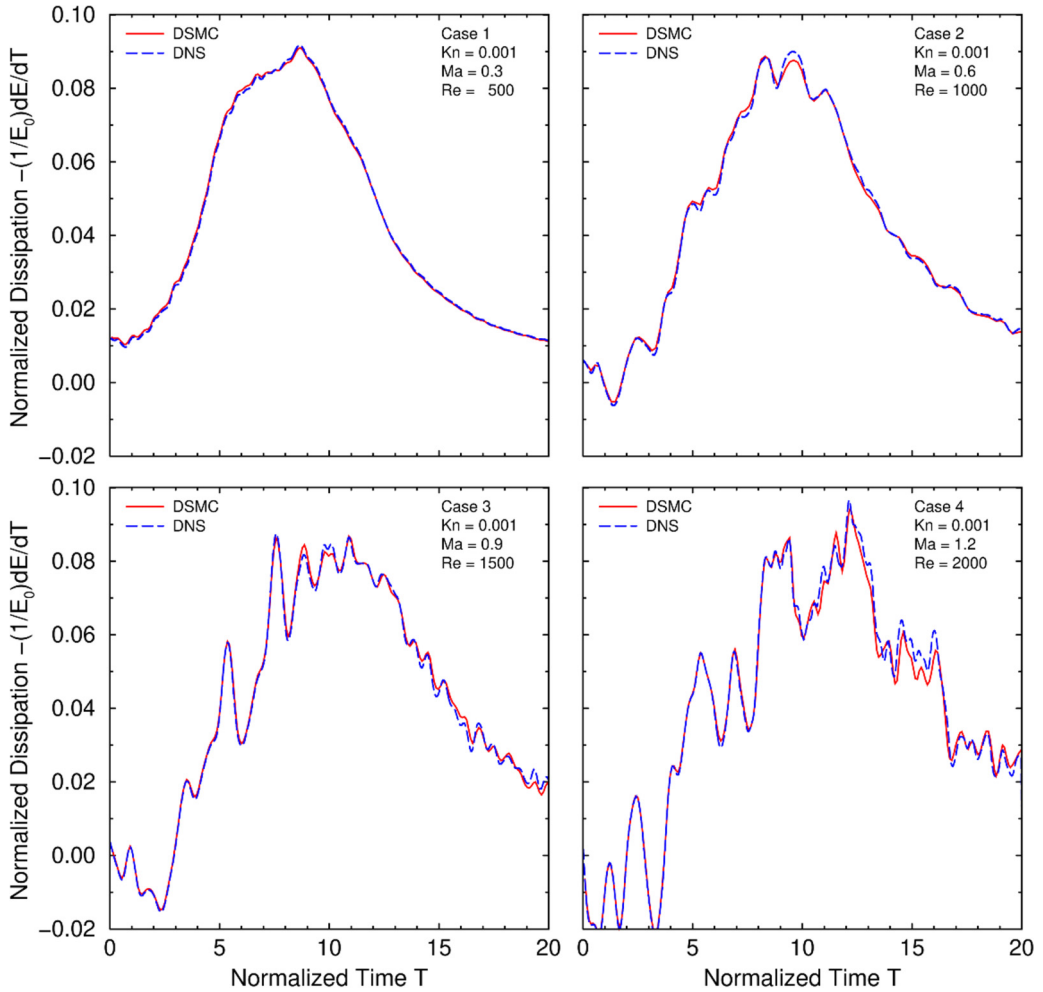


FIG. 2. Dissipation versus time from DSMC and DNS.

processes, especially molecular-level fluctuations, are not having a significant effect on the overall energy decay for these near-continuum conditions although they may be affecting the fine details of how the flow evolves from its initial conditions to the turbulent state.

B. Velocity fields

Figures 4–11 present plots of the u velocity component on the bounding faces of the domain from DSMC and DNS at two times: near the maximum dissipation time and much later. The top face (the y – z plane $x = \pi L$) is plotted below each perspective image using an expanded scaling to allow easier comparison of the flow fields on this face. The u velocity component on the top face is singled out for special attention because this quantity should remain equal to zero as long as the symmetries of the initial conditions are preserved as the flow evolves in time [11,12].

Except for being slightly noisy, the DSMC molecular results for all four cases are virtually identical to the corresponding DNS Navier-Stokes results before the maximum dissipation time. At that time, large-scale structures that are the remnants of the initial conditions are clearly discernible, but smaller-scale structures are also present. In particular, the large-scale and small-scale features of

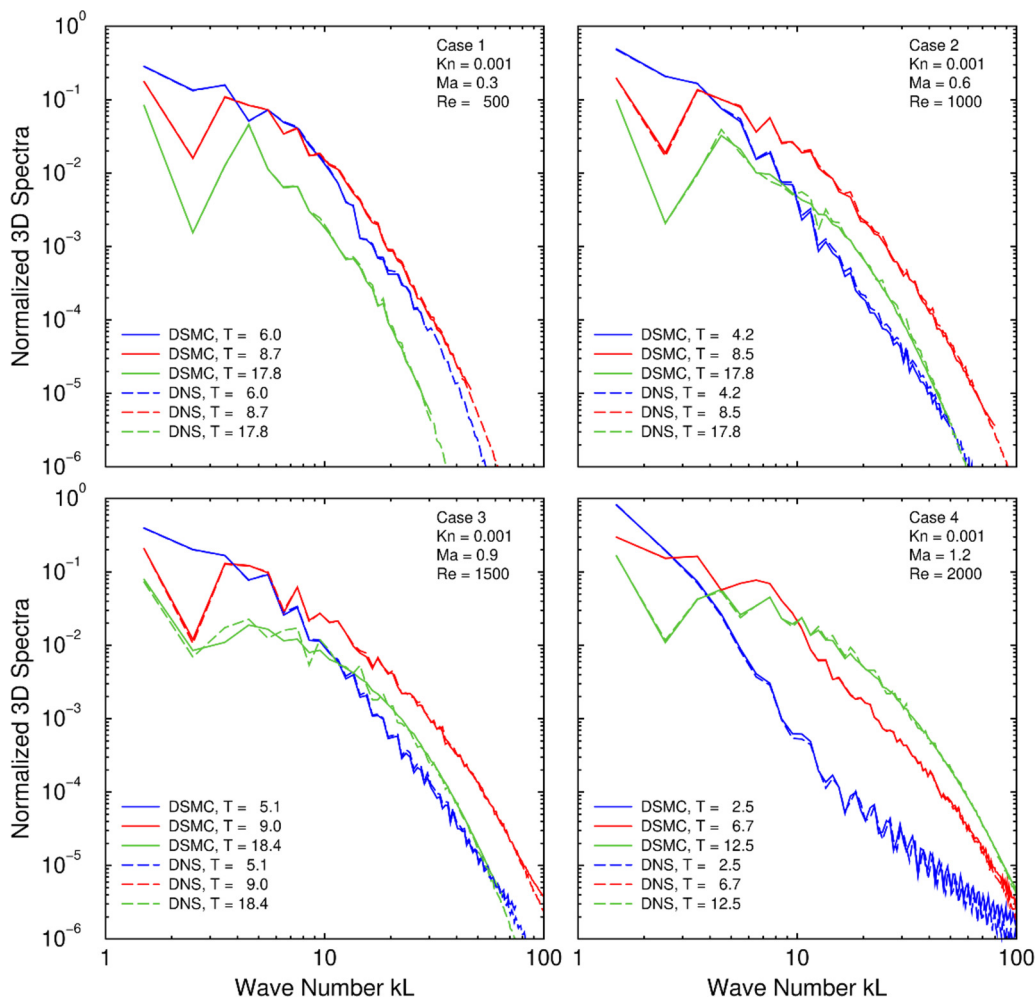


FIG. 3. Spectra at selected times from DSMC and DNS.

the DSMC and DNS flow fields preserve the symmetry and antisymmetry features that are present in the initial conditions. At later times, this statement still applies roughly for case 1 but no longer applies for cases 2–4. More specifically, although the DNS flow fields preserve these features, the DSMC flow fields do not. This is seen most clearly on the top face: The DSMC flow fields exhibit large velocity fluctuations, but the corresponding DNS flow fields have negligibly small velocity fluctuations.

The velocity fluctuations observed in the flow fields shown in Figs. 4–11 are quantified in the following manner. The rms value of the u velocity component on the top face is computed at several times before and after the maximum dissipation time for both methods and all four cases. Figure 12 presents the resulting values as functions of Reynolds number (see Table I) and time. The DSMC and DNS results exhibit different trends. Although the DSMC molecular fluctuations are basically the same for all cases and times, the DSMC velocity fluctuations grow significantly in amplitude with increasing Reynolds number and with time near the maximum dissipation time. In contradistinction, the DNS velocity fluctuations are small for all Reynolds numbers and do not grow significantly in amplitude near the maximum dissipation time.

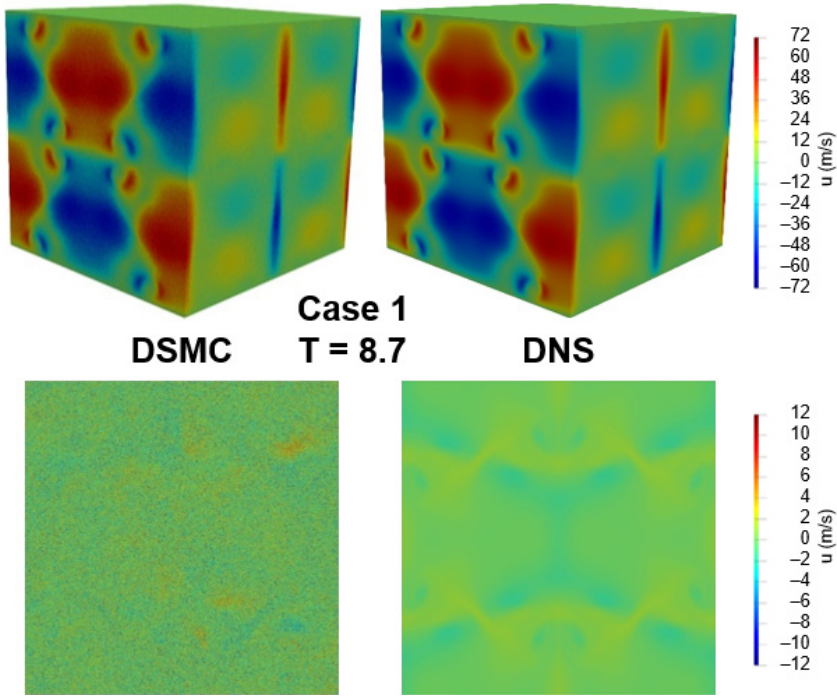


FIG. 4. Case 1: u velocity at $T = 8.7$. Squares are top plane ($x = \pi L$).

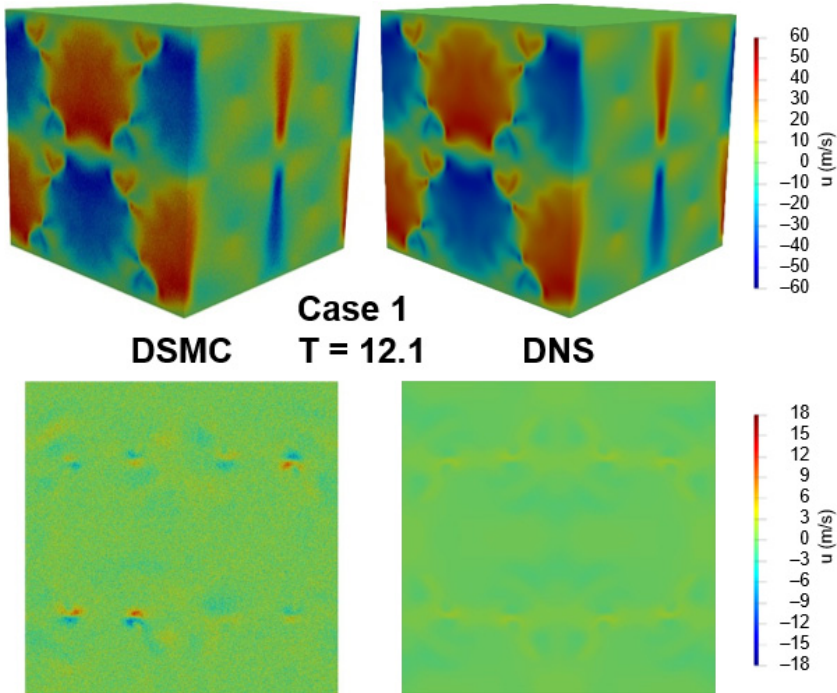


FIG. 5. Case 1: u velocity at $T = 12.1$. Squares are top plane ($x = \pi L$).

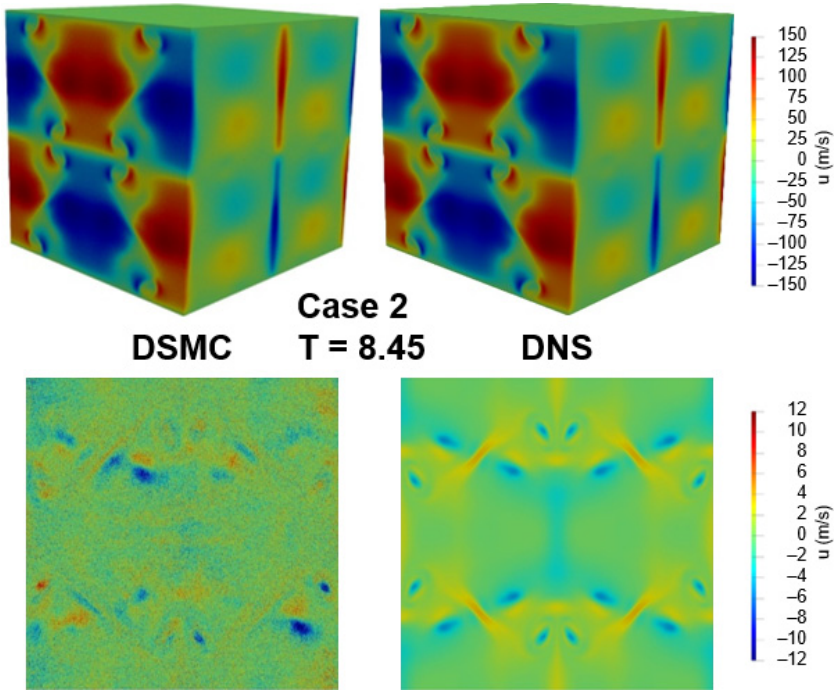


FIG. 6. Case 2: u velocity at $T = 8.45$. Squares are top plane ($x = \pi L$).

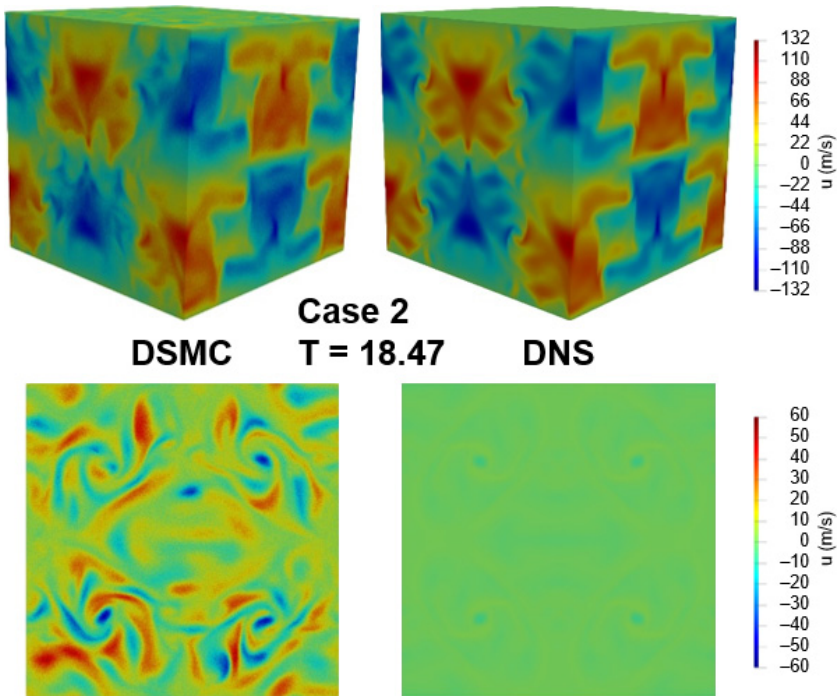


FIG. 7. Case 2: u velocity at $T = 18.47$. Squares are top plane ($x = \pi L$).

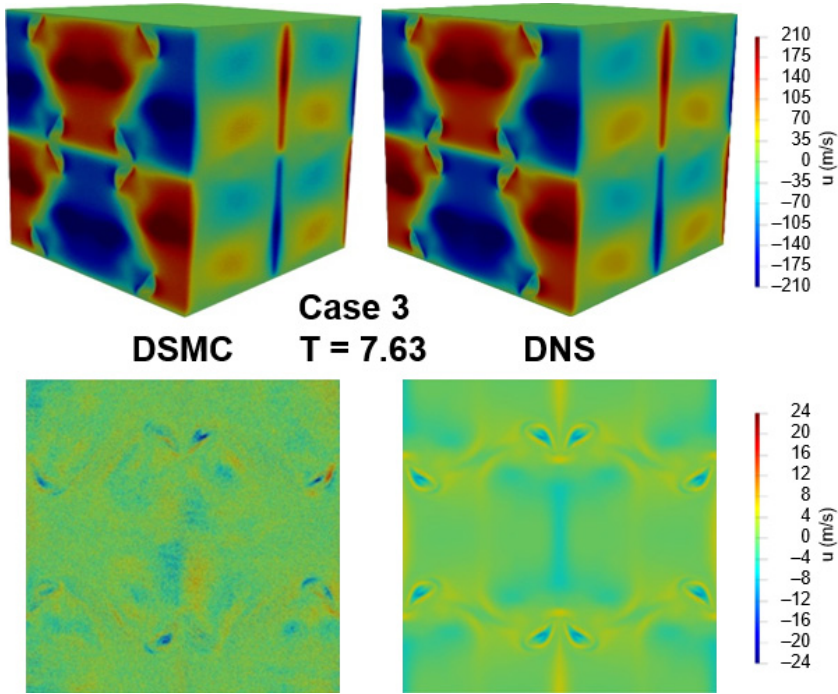


FIG. 8. Case 3: u velocity at $T = 7.63$. Squares are top plane ($x = \pi L$).

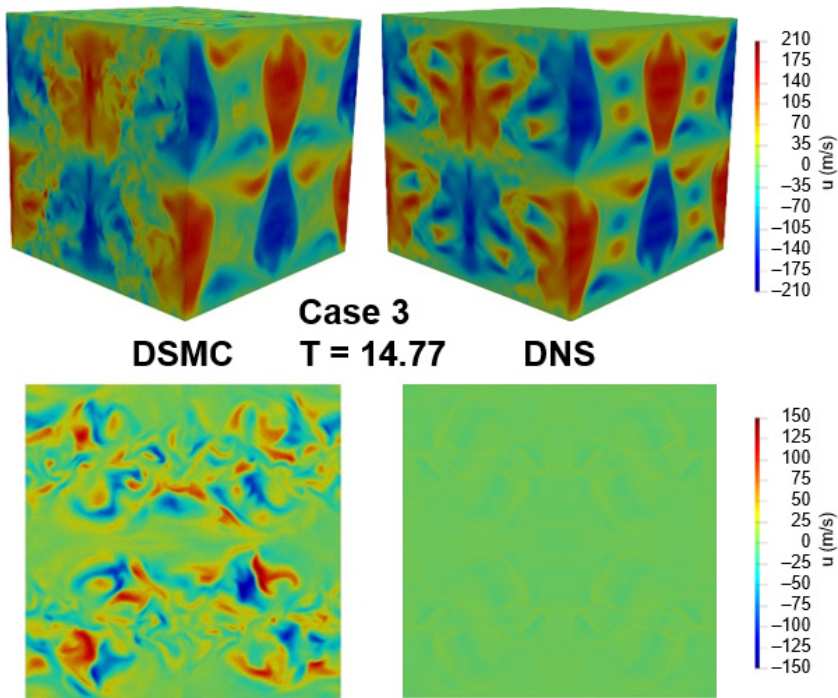


FIG. 9. Case 3: u velocity at $T = 14.77$. Squares are top plane ($x = \pi L$).

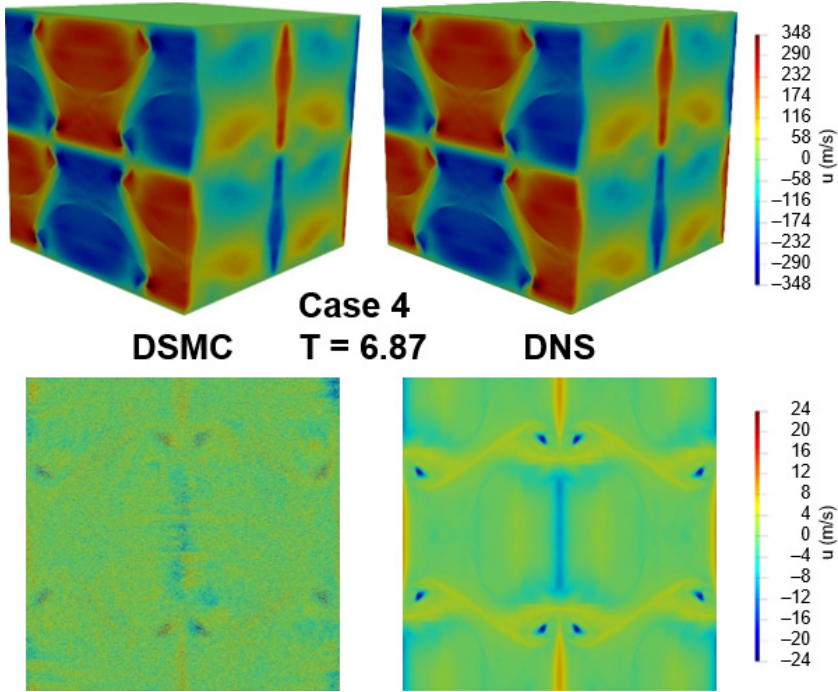


FIG. 10. Case 4: u velocity at $T = 6.87$. Squares are top plane ($x = \pi L$).

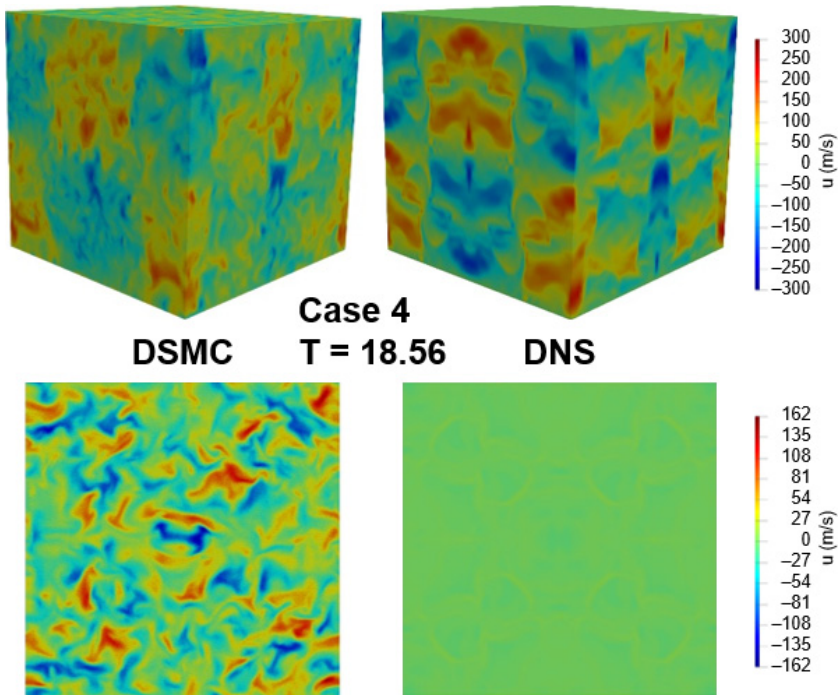


FIG. 11. Case 4: u velocity at $T = 18.56$. Squares are top plane ($x = \pi L$).

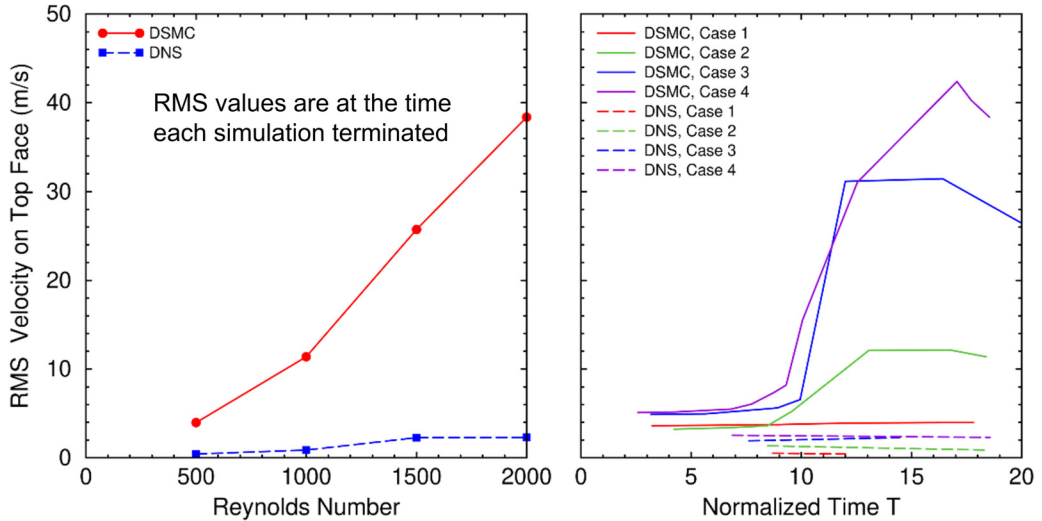


FIG. 12. Rms u velocity on the top face versus Reynolds number (left) and time (right).

Although extreme velocity fluctuations at Kolmogorov and sub-Kolmogorov length scales have been observed in some high-resolution DNS simulations [4,5], the magnitude of the velocity fluctuations observed in the present DSMC simulations suggests that they have a different origin. The following scenario is suggested to explain the above results. Molecular fluctuations break symmetries and take the flow field down a different but basically similar trajectory through phase space from the initial flow conditions to the turbulent flow field. This suggestion is motivated by the fact that molecular fluctuations are inherently present in the DSMC (MGD) simulations but are absent from the DNS (CFD) simulations. The fact that these velocity fluctuations grow with time supports this assertion. Moreover, symmetry breaking induced by molecular fluctuations is significant for the Richtmyer-Meshkov and the Rayleigh-Taylor instabilities [24,25].

Before the maximum dissipation time, the DSMC and DNS flow fields are almost identical. This is probably because the smallest length scales are larger than the Kolmogorov length scale, so the flow fields are continuum even at the smallest length scales that are present at these times. Hence, molecular fluctuations are of minimal importance, so symmetry and antisymmetry features are preserved. For case 1, this situation applies at all times, but, for cases 2–4 at late times (well past the maximum dissipation time), the DSMC and DNS flow fields exhibit differences (e.g., the u velocity component on the top face). This is probably because the smallest length scales are comparable to the Kolmogorov length scale, so the flow fields are noncontinuum at the smallest length scales present at these times. Hence, molecular fluctuations that exist at these small scales are no longer negligible, and, as a result, symmetry and antisymmetry features are broken.

V. PHYSICAL OR NUMERICAL?

Since each DSMC particle actually represents a large number of real gas molecules rather than a single real gas molecule, the level of molecular fluctuations in a DSMC simulation is much higher than in a real gas. If a one-to-one correspondence between DSMC particles and real gas molecules could be achieved, the level of molecular fluctuations would be physically realistic, but this situation is typically not possible to achieve in practice. However, if the sample size could be increased substantially, then the level of molecular fluctuations could be reduced. Since every time that a molecule moves or collides it represents a different point in six-dimensional phase space, the sample size can be increased by averaging over times that are long compared to the time step but are

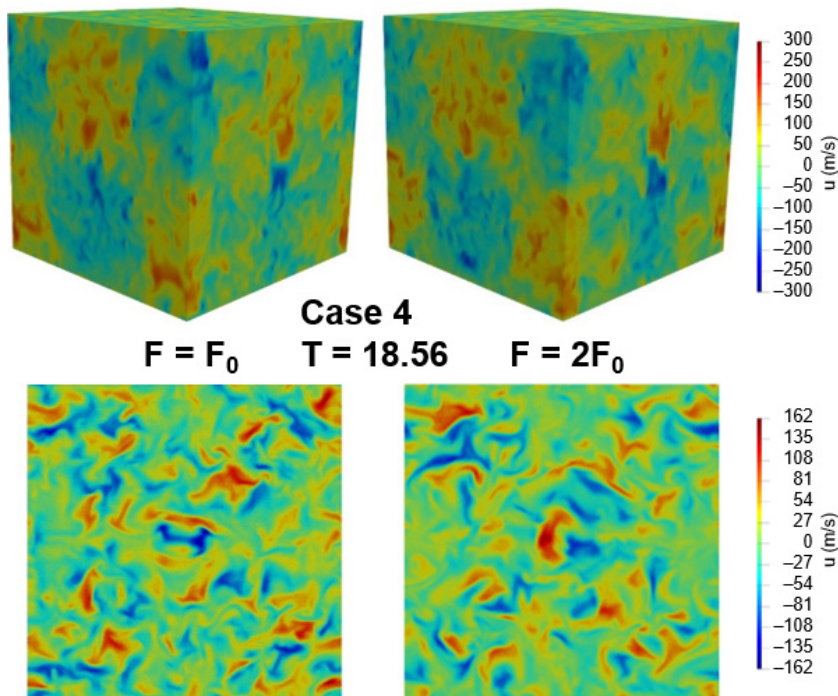


FIG. 13. DSMC u velocity fields for case 4 at $T = 18.56$ with two different values of the simulation ratio: nominal $F = F_0$ (left) and twice nominal $F = 2F_0$ (right).

short compared to the shortest flow timescales (here, the Kolmogorov timescale). If the sample size is close to the simulation ratio F (the number of real gas molecules represented by one DSMC particle), the level of real molecular fluctuations in the real gas can be realized [14].

Thus, it is important to investigate the effect of the simulation ratio on the DSMC results. As the simulation ratio F is decreased, a DSMC simulation represents the real gas more closely. The simulations previously presented are performed with a simulation ratio of $F = F_0 = 16\,000$. Here, additional simulations are performed with a simulation ratio of $F = 2F_0 = 32\,000$ (i.e., twice the original value). Figure 13 shows results from these two simulations for case 4 at $T = 18.56$. The two flow fields are quite similar (except for noise). Although the u velocity fields on the top face differ in detail (as expected for different paths through the phase space of a chaotic system), they have similar rms values: 38 m/s for $F = F_0$ and 36 m/s for $F = 2F_0$, which are two orders of magnitude larger than their corresponding means. At this late time, both flow fields lack the symmetry and antisymmetry features that characterize their initial conditions and their flow fields well before the time of maximum dissipation. These observations suggest that the role of molecular fluctuations is not affected significantly by the simulation ratio.

Recent DSMC simulations of the Richtmyer-Meshkov instability (RMI) [24] and the Rayleigh-Taylor instability (RTI) [25] provide additional support for this assertion. In the RMI, molecular fluctuations in the DSMC simulations are observed to trigger secondary instabilities that break symmetries which are preserved in the corresponding DNS simulations but which are broken in corresponding experiments. In the RTI, molecular fluctuations in the DSMC simulations are observed to trigger both the instability itself and secondary instabilities without an artificially imposed initial perturbation and thereby produce values for the most unstable wavelength and the growth rate that agree closely with experiments and that are independent of the initial conditions.

VI. CONCLUSIONS

The molecular-gas-dynamics simulations presented here provide the first investigation of molecular-level effects on the energy decay of turbulent flows in the near-continuum regime. The direct simulation Monte Carlo (DSMC) method (noncontinuum molecular gas dynamics) and direct numerical simulation (DNS) of the Navier-Stokes equations (continuum computational fluid dynamics) are used to simulate compressible Taylor-Green vortex flow at near-continuum flow conditions. For the Mach and Reynolds numbers examined, both methods produce basically the same energy decay. However, the molecular fluctuations in DSMC (and in experiments) can break symmetries, which in turn can cause the flows to evolve along trajectories in phase space that are different from but basically similar to those of DNS, which lacks molecular fluctuations. This appears to be the main difference between continuum and near-continuum turbulent flow. The present investigation is focused on the energy history in a freely decaying turbulent flow. Future investigations could focus on similar issues in sustained turbulence for wall-bounded flows, for which slip at the wall might introduce additional effects.

ACKNOWLEDGMENTS

The authors thank Timothy P. Koehler and Ryan M. McMullen of Sandia National Laboratories for helpful discussions about this research and its presentation herein.

Sandia National Laboratories is a multimission laboratory managed and operated by National Technology and Engineering Solutions of Sandia, LLC, a wholly owned subsidiary of Honeywell International, Inc., for the U.S. Department of Energy's National Nuclear Security Administration under contract DE-NA0003525.

This paper describes objective technical results and analysis. Any subjective views or opinions that might be expressed in the paper do not necessarily represent the views of the U.S. Department of Energy or the United States Government.

This manuscript has been authored by National Technology and Engineering Solutions of Sandia, LLC, under Contract No. DE-NA0003525 with the U.S. Department of Energy. The United States Government retains and the publisher, by accepting the article for publication, acknowledges that the United States Government retains a non-exclusive, paid-up, irrevocable, world-wide license to publish or reproduce the published form of this manuscript, or allow others to do so, for United States Government purposes.

-
- [1] G. K. Batchelor, *The Theory of Homogeneous Turbulence* (Cambridge University Press, Cambridge, 1953).
 - [2] K. R. Sreenivasan and R. A. Antonia, The phenomenology of small-scale turbulence, [Annu. Rev. Fluid Mech. **29**, 435 \(1997\)](#).
 - [3] J. Schumacher, J. D. Scheel, D. Krasnov, D. A. Donzis, V. Yakhot, and K. R. Sreenivasan, Small-scale universality in fluid turbulence, [Proc. Natl. Acad. Sci. USA **111**, 10961 \(2014\)](#).
 - [4] D. Buaria, A. Pumir, E. Bodenschatz, and P. K. Yeung, Extreme velocity gradients in turbulent flows, [New J. Phys. **21**, 043004 \(2019\)](#).
 - [5] J. Schumacher, Sub-Kolmogorov-scale fluctuations in fluid turbulence, [Europhys. Lett. **80**, 54001 \(2007\)](#).
 - [6] S. Stefanov, I. D. Boyd, and C.-P. Cai, Monte Carlo analysis of macroscopic fluctuations in a rarefied hypersonic flow around a cylinder, [Phys. Fluids **12**, 1226 \(2000\)](#).
 - [7] E. R. Van Driest, Turbulent boundary layer compressible fluids, [J. Aeronaut. Sci. **18**, 145 \(1951\)](#).
 - [8] E. R. Van Driest, Turbulent boundary layer on a cone in a supersonic flow at zero angle of attack, [J. Aeronaut. Sci. **19**, 55 \(1952\)](#).
 - [9] H. Tennekes and J. L. Lumley, *A First Course in Turbulence* (The MIT Press, Cambridge, MA, 1972).
 - [10] U. Frisch, *Turbulence: The Legacy of A. N. Kolmogorov* (Cambridge University Press, Cambridge, 1996).

- [11] G. I. Taylor and A. E. Green, Mechanism of the production of small eddies from large ones, *Proc. R. Soc London, Ser. A* **158**, 499 (1937).
- [12] M. E. Brachet, D. I. Meiron, S. A. Orszag, B. G. Nickel, R. H. Morf, and U. Frisch, Small-scale structure of the Taylor-Green vortex, *J. Fluid Mech.* **130**, 411 (1983).
- [13] G. A. Bird, *Molecular Gas Dynamics and the Direct Simulation of Gas Flows* (Clarendon Press, Oxford, 1998).
- [14] A. L. Garcia, Nonequilibrium fluctuations studied by a rarefied gas simulation, *Phys. Rev. A* **34**, 1454 (1986).
- [15] M. A. Gallis, N. P. Bitter, T. P. Koehler, J. R. Torczynski, S. J. Plimpton, and G. Papadakis, Molecular-Level Simulations of Turbulence and Its Decay, *Phys. Rev. Lett.* **118**, 064501 (2017).
- [16] M. A. Gallis, T. P. Koehler, and S. J. Plimpton, SPARTA stochastic particle real time analyzer validation and verification test suite, Sandia Report No. SAND2014-19198 (2014).
- [17] S. J. Plimpton, S. G. Moore, A. Borner, A. K. Stagg, T. P. Koehler, J. R. Torczynski, and M. A. Gallis, DSMC on petascale machines and beyond, *Phys. Fluids* **31**, 086101 (2019).
- [18] G. A. Bird, M. A. Gallis, J. R. Torczynski, and D. J. Rader, Accuracy and efficiency of the sophisticated direct simulation Monte Carlo algorithm for simulating noncontinuum gas flows, *Phys. Fluids* **21**, 017103 (2009).
- [19] M. Howard, A. M. Bradley, S. W. Bova, J. R. Overfelt, R. M. Wagnild, D. J. Dinzl, M. F. Hoemmen, and A. Klinvex, Towards a performance portable compressible CFD code, AIAA-2017-4407 (American Institute of Aeronautics and Astronautics, Reston, VA, 2017).
- [20] J. B. Maeng, T. C. Fisher, and M. H. Carpenter, Generalized entropy stable weighted essentially non-oscillatory finite difference schemes in multi-block domains, AIAA-2019-3205 (American Institute of Aeronautics and Astronautics, Reston, VA, 2019).
- [21] G. V. Candler, H. B. Johnson, I. Nompelis, P. K. Subbareddy, T. W. Drayna, V. Gidzak, and M. D. Barnhardt, Development of the US3D code for advanced compressible and reacting flow simulations, AIAA-2015-1893 (American Institute of Aeronautics and Astronautics, Reston, VA, 2015).
- [22] R. W. MacCormack and G. V. Candler, The solution of the Navier-Stokes equations using Gauss-Seidel line relaxation, *Comput. Fluids* **17**, 135 (1989).
- [23] P. K. Subbareddy and G. V. Candler, A fully discrete, kinetic energy consistent finite-volume scheme for compressible flows, *J. Comput. Phys.* **228**, 1347 (2009).
- [24] M. A. Gallis, T. P. Koehler, J. R. Torczynski, and S. J. Plimpton, Direct simulation Monte Carlo investigation of the Richtmyer-Meshkov instability, *Phys. Fluids* **27**, 084105 (2015).
- [25] M. A. Gallis, T. P. Koehler, J. R. Torczynski, and S. J. Plimpton, Direct simulation Monte Carlo investigation of the Rayleigh-Taylor instability, *Phys. Rev. Fluids* **1**, 043403 (2016).